Numerical investigation of separation pattern and separation pattern transition in overexpanded single expansion ramp nozzle

Y. Yu, J. Xu*, J. Mo and M. Wang
xujl@nuaa.edu.cn
Jiangsu Province Key Laboratory of Aerospace Power System
Nanjing University of Aeronautics and Astronautics
China

ABSTRACT

Flow separation results in many problems to single expansion ramp nozzle (SERN) and hypersonic vehicle. However, little research has been conducted on the separation patterns and their effects on SERN's performance. In the present paper, the numerical simulation is adopted to get the intuitive results and help to analyse the separation phenomena in SERN thoroughly. The main separation pattern is the restricted shock separation (RSS) in SERN, and the free shock separation (FSS) only appears in a small range of the nozzle pressure ratio (*NPR*), which is much different from the axisymmetric rocket nozzle. Further CFD results show that the separation pattern transition makes great effects on the performance of SERN, especially the lift. Moreover, the performance of SERN has an extreme in the separation pattern transition because of the main jet impinging on the expansion ramp. The transitions occur in both the startup and shutdown processes but the critical nozzle pressure ratios of the separation pattern transitions are different, which leads to a hysteresis loop of SERN performance.

Paper No. 3967. Manuscript received 1 March 2013, revised version received 29 November 2013, accepted 1 December 2013.

https://doi.org/10.1017/S0001924000009192 Published online by Cambridge University Press

NOMENCLATURE

CFD	computational fluid dynamics
FSS	free shock separation
H_e	height of the exit
H_t	height of the throat
MOC	method of characteristic
NPR	nozzle pressure ratio
P	static pressure
P_a	ambient pressure
P_t	total pressure
qRSS	quasi-restricted shock separation
RBCC	rocket based combined cycle
RSS	restricted shock separation
RSS(flap)	restricted shock separation with separation bubble forming on flap
RSS(ramp)	restricted shock separation with separation bubble forming on ramp
SERN	single expansion ramp nozzle
T	static temperature
T_t	total temperature
TBCC	turbine-based combined cycle
TIC	truncated ideal contour
TOC	thrust optimised contour
TOP	thrust optimised parabolic
UDF	user defined function
X	x co-ordinate
Y	y co-ordinate

1.0 INTRODUCTION

Flow separation in the nozzle will appear when the vehicle flies at a low Mach number, and the nozzle works under a serious over-expanded condition. The flow separation in nozzles is undesirable because it can lead to critical unsteady force, which might threaten the safety of the vehicle, and damage the nozzle. Several separation patterns might exist in a nozzle, which is usually designed under a high pressure ratio condition. In addition, the specific separation pattern always occurs in a definite range of nozzle pressure ratio (*NPR*), which is the ratio of the total pressure at the inlet of the nozzle to the back pressure. Moreover, the separation patterns have their own special forms and make different influences on the performance of the nozzle. During the startup or shutdown process, the operating *NPR* changes continuously, so the different separation patterns might occur in sequence, but the performance changes suddenly and intensively during the separation pattern transition processes, which can reduce the life time and the stability of the nozzle.

With the development of hypersonic vehicle, the flight Mach number range becomes much wider and the combined cycle engines, such as the TBCC (turbine-based combined cycle) and RBCC (rocket-based combined cycle), are regarded as the most promising propulsion system for the future. SERN (single expansion ramp nozzle) is often adopted on hypersonic vehicle because of its better adaptability and lightness of the structure. The simplified scramjet schematic diagram is shown in Fig. 1 and the sketch of vehicle afterbody equipped with SERN is shown in Fig. 2. The afterbody of the vehicle is a part of the SERN which offers a good integration into the aircraft

https://doi.org/10.1017/S0001924000009192 Published online by Cambridge University Press

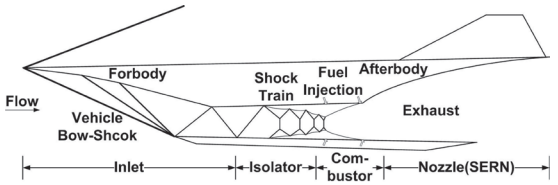

Figure 1. Simplified scramjet schematic diagram.

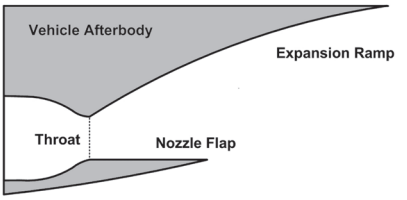

Figure 2. Sketch of vehicle afterbody equipped with SERN.

and have a certain self-adapt ability at off-design operation[1]. The TBCC engine uses the turbojet propulsion part from take-off to approximately Mach 4, then the engine transfers to the ramjet/scramjet propulsion system for the increased velocities[2]. The SERN adopted on TBCC is always designed at high Mach number, but at low flight Mach number, SERN performance is greatly influenced by flow separation and the location of separation point[3].Therefore, the separation in SERN is a key problem when the TBCC engine works at low speed.

The flow fields of the over-expanded SERN had been show by Xu[4] with PIV experiment, and the numerical simulation method had been validated in his study. In the PIV experimental results, the structure of the shock waves had been shown clearly and the separation bubble could be observed easily. The k-ε turbulence model was adopted in the numerical simulation. Gamble and Haid[5] discussed the performance of the off-design SERN and tried to improve the performance by using fluidic injection. In their study, two kinds of separation patterns would occur in SERN. The first mechanism was free shock separation (FSS). This occurred in over-expanded nozzles when the compression required to bring the boundary layer flow at the trailing edge of the nozzle up to ambient conditions induces boundary layer separation[5]. The second mechanism was shock-induced separation (SIS). This occurred when a shock impinges on the SERN ramp surface and resulted in a pressure increase sufficient to separate the flow[5]. Fluidic injection had been shown to improve nozzle performance at off-design flight conditions. The shock accomplished by injecting fluid traversed the gas path, impinged on the SERN ramp, and induced separation to decrease the drag due to over-expansion. The prediction of the separation point was also a difficult problem in over-expanded nozzles. Schmucker presented a separation criterion based on the axisymmetric rocket nozzle, but the criterion was not fully suitable for SERN. Ge[6] revised the criterion and it made a good prediction of the separation for SERN.

The various separation patterns were firstly found in rocket nozzles about 60 years ago. In intensive study, the characteristics of different separation patterns were revealed and the separation pattern transitions were found in the processes of startup and shutdown. In the early 1950s and 1960s, the free shock separation (FSS) in nozzles was reported in many publications[7]. In FSS, the main jet did not reattach to the wall after the separation, just like the behaviour of the free jet downstream the separation point. According to the literature[7], the FSS was the most common separation pattern in axisymmetric rocket nozzle. In 1973, a new separation pattern, restricted shock separation (RSS), was found in the experiment of the subscale model of J-2S, for which the flow reattached to the wall downstream the separation point and formed a closed recirculation bubble[8]. For a long time, it was considered that RSS only occurred in subscale experiment with cold air, but it was proven later that RSS could also appear in full-scale nozzles and hot conditions[9]. After that, the separation pattern transition and its effects on the nozzle performance have been concerned by more and more researchers[10-25].

https://doi.org/10.1017/S0001924000009192 Published online by Cambridge University Press

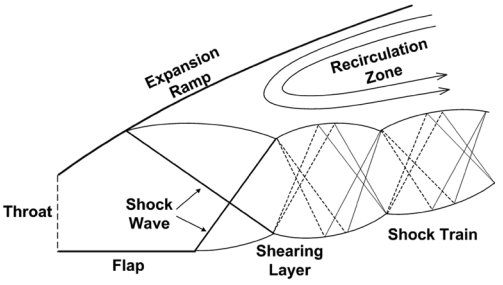

(a) Sketch of FSS in short flap SERN

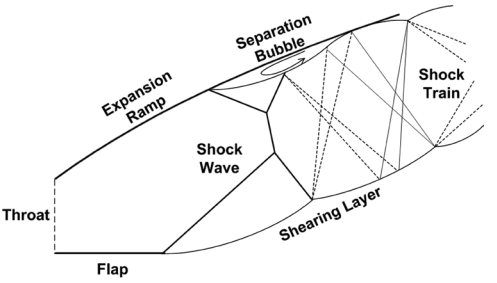

(b) Sketch of RSS in short flap SERN

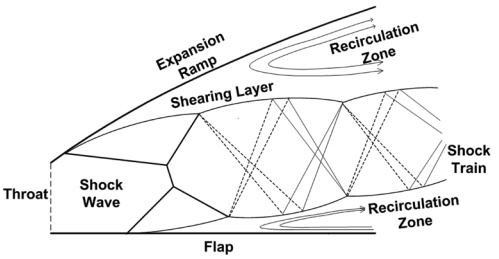

(c) Sketch of FSS in long flap SERN

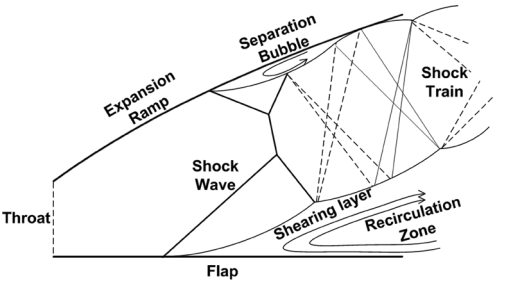

(d) Sketch of RSS in long flap SERN, separation bubble on expansion ramp

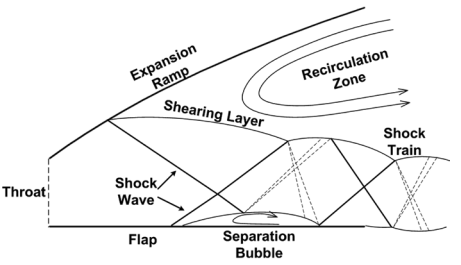

(e) Sketch of RSS in long flap SERN, separation bubble on flap

Figure 3. The sketches of various separation patterns in SERN.

The flow separation and various separation patterns appear as well when SERN is operating under over-expanded condition, which were observed when the nozzle worked in the processes of startup and shutdown. Figure 3 shows the sketches of various separation patterns in SERN. In Ref. 10, it has been pointed out that FSS is the most common separation pattern in the rocket nozzle and RSS just occurs in a few special kinds of contours. However, in SERN, it is obviously that the RSS is the most common separation pattern, while the FSS in the SERN is not a very stable status and only appears in a quite narrow *NPR* range. Comparing with the characteristics of separation patterns in axisymmetric rocket nozzle, the *NPR* of FSS in SERN is lower than that in rocket nozzles, and there is no strong normal shock wave in SERN, only the oblique separation shock waves appear. On the contrary, the Mach disk is the main shock wave of FSS in rocket nozzles, and there is a recirculation zone after the Mach disk, which is encircled by the shock train

https://doi.org/10.1017/S0001924000009192 Published online by Cambridge University Press

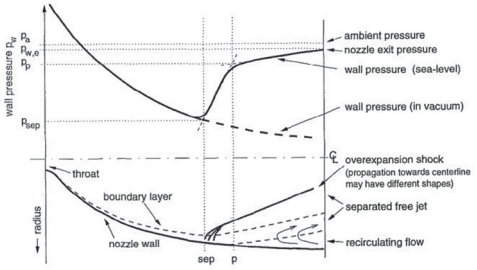

Figure 4. FSS phenomenological sketch[10].

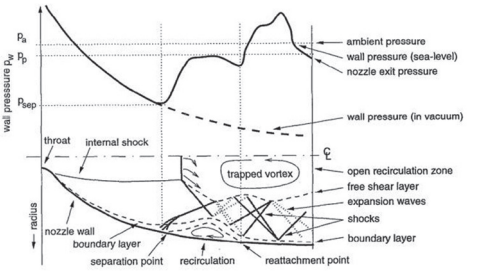

Figure 5. RSS phenomenological sketch[10].

downstream of the separation shock. When SERN works in RSS, the flow is restricted on one side, and the recirculation zone is filled by ambient air and appears on the other side. But when the rocket nozzle works in RSS, the flow behind the separation shock waves will all reattach to the wall. There are two kinds of RSS in SERN with long flap, and the *NPR* corresponding to the separation bubble forming on the expansion ramp status is much higher than that of the separation bubble forming on the flap.

The separation pattern transition from FSS to RSS during the startup process, and from RSS to FSS during the shutdown processes of rocket nozzle, have been found[10-13]. Because side loads were always observed during the startup and shutdown process, it was naturally to associate the side load with separation pattern transition. Frey and Hagemann[10-13] made a series of researches on flow separation prediction, flow separation pattern transition and side loads in rocket nozzles. They pointed out five potential origins altogether for side load, and considered the separation pattern transition in nozzles as the main origin[10]. In the paper, the process of the separation pattern transition in the rocket nozzle was described, and it was shown that the critical transition *NPR* from RSS to FSS during the shutdown process was lower than the one from FSS to RSS during the startup. Figures 4 and 5 show the phenomenological sketch of FSS and RSS in rocket nozzle respectively.

Because the flow separation could affect the performance of rocket nozzle, more and more researchers kept their eyes on separation patterns and their transitions in it. Firstly, the flow separation would cause serious problems to the performance and the structure of the nozzle. For example, in the test of LE-7A engine[14] which is the main-stage cryogenic liquid rocket engine of the H-IIA launch vehicle, the large side loads and the damage of some regenerative cooling tubes were found during the nozzle startup and shutdown process. It was presumed that the side load peak was caused by separation pattern transition, and the damage of regenerative cooling tubes was resulted by the reattachment of the RSS. Watanabe[15] tried to use a cooling step inside the nozzle to reduce the side load caused by the separation transition, but it could not solve the problems fundamentally. Secondly, the separation patterns and their transitions phenomena were very complex, which would vary depending on the different expansion wall profiles and the operating *NPR* of the axisymmetric nozzle. For example, Nasuti[16] simulated the separation patterns in the nozzles with three different profiles, shown as Fig. 6, namely the truncated ideal contour (TIC), thrust optimised contour (TOC) and thrust optimised parabolic (TOP). From the analysis of the separation patterns, it was found that only in the TOP contour nozzle both RSS and FSS separation patterns appeared, and only FSS appeared in the TOC and TIC contour nozzles for all the *NPR*s, because the Mach disks in the TOC and TIC contour nozzles were less curved than that

https://doi.org/10.1017/S0001924000009192 Published online by Cambridge University Press

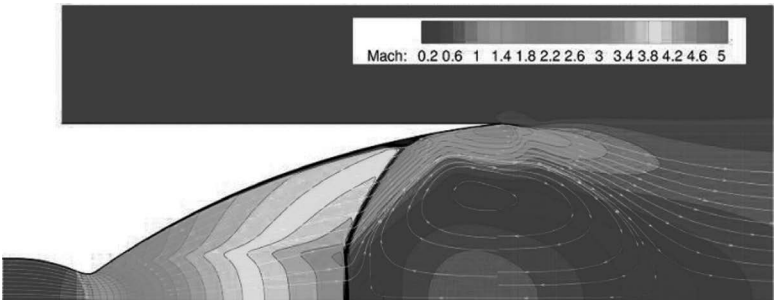

(a) TOP contour, RSS, operating *NPR* = 30

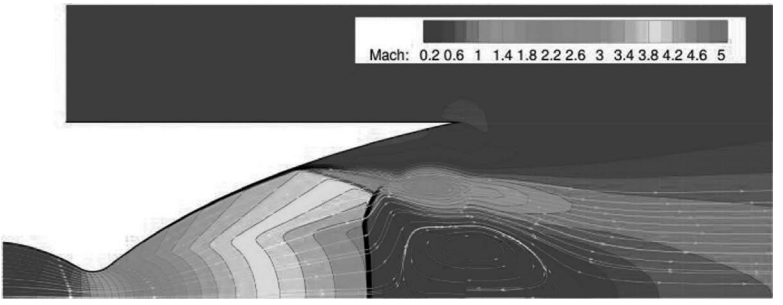

(b) TOC contour, FS, operating *NPR* = 30

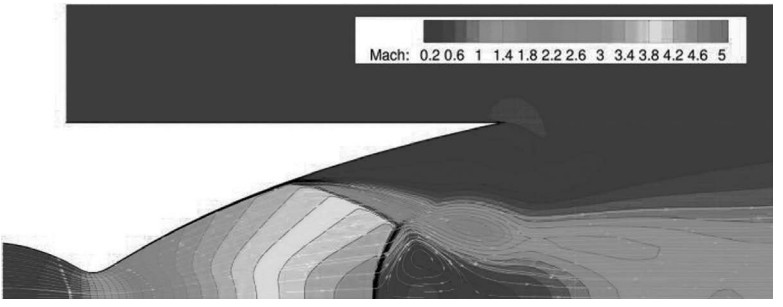

(c) TIC contour, FS, operating *NPR* = 30

Figure 6. Results of numerical simulation, TOP, TOC and TIC, reproduced from Nasuti[16].

in the TOP nozzle. Furthermore, the quasi-restricted shock separation (qRSS) was discovered by Kwan and Stark[17]. From the CFD results, a special status in startup process was observed that RSS only occurred in part of the nozzle, and the nozzle would become fully RSS soon if the *NPR* was increased continuously, and this status was named as qRSS. Wang[18,19] simulated the process of separation pattern transition in 2D and 3D by CFD method. The unsteady process of the transition in startup was showed and the changes of the side load were captured by the numerical simulation.

Besides the numerical simulation method, a lot of experiments of over expanded rocket nozzle have been conducted in recent years. Reijasse *et al*[20] analysed the experimental results of subscale model of TIC and TOC, discussed the characteristics of the nozzle operating under the over expanded condition, and showed the unsteadiness of the pressure distribution on the wall. Verma,

https://doi.org/10.1017/S0001924000009192 Published online by Cambridge University Press

S.B. and Haidn, O. *et al*[21] discussed the qRSS in subscale TOP contour model. Brown[22, 16] used the Quasi-Static Strain-Gage to measure the side load of the nozzle and studied the effect of the flow separation on the nozzle. Ruf[23,24] tested the separation pattern transition process from FSS to RSS, then to FSS again, and the pressure distribution on the wall was given. Baars[25] measured the changes of the side load and analysed its unsteady characteristics.

The separation pattern transition in rocket nozzle can cause the side load which will result in the serious control problem to rocket and can damage the structure. There are various separation patterns in SERN and the separation pattern transition exists in SERN as well, but the force caused by the transition, which is called side loads in rocket nozzle, is on the direction of lift in SERN. So the SERN performance has a suddenly change when the separation patterns transition happens, which is a great challenge to the structural strength and the control system. There is a large Mach disk when the rocket nozzle works in FSS and RSS, so only a little part of the jet, which is behind the separation shock and near the wall, is influenced by separation pattern transition. However, in SERN, there is no or very little normal shock wave when SERN works in FSS and RSS, therefore, the flow field changes greatly during the separation pattern transition. Moreover, the direction of the jet of SERN also changes during the process of separation pattern transition. In general, the separation pattern transition makes more serious influences on the performance of SERN than of rocket nozzle.

Although the flow separation can result in many problems to SERN and hypersonic vehicle's performance, the separation pattern and the separation pattern transition have not attracted much attention of the researchers yet. In the following, the characteristics of the SERN separation pattern, which are different from rocket nozzle, and the effects of the separation pattern transition on the SERN performance will be discussed. Furthermore, the unsteady CFD simulation was conducted to study the hysteresis loop of the SERN performance occurring in the startup and shutdown process of the SERN.

2.0 SEPARATION PATTERNS IN THE EXPERIMENT OF SERN

2.1 Test facilities

The test is made in the Internal Flow Research Center of Nanjing University of Aeronautics and Astronautics (NUAA). It is a cold blow down wind tunnel and the size of the cubic vacuum chamber is 1·8m × 1·7m × 1·7m. Test air is supplied from a high pressure vessel and the maximum stagnation pressure ranges from 0·4 to 0·6MPa. The low ambient pressure is supplied by vacuum pump and the back pressures range from 0·02 to 0·05MPa. Quartz windows are installed in the opposite walls of the test section for Schlieren and other nonintrusive techniques. The Schlieren system is a two-concave-mirror system and the diameter of the mirror is 150mm. The high definition videos and images can be taken by this system. The error of the pressure transducer used in the test system is 0·05%. The sketch and photograph of the test facility is shown in Fig. 7 and Fig. 8, respectively.

Figure 9 shows the SERN model tested in the experiment, and the photo of the SERN model installed in the wind tunnel is shown in Fig. 10. The area of the throat is 419·9mm^2 and the area of the exit is 1290·58mm^2. The aspect ratio of the throat is 2·5. The length of the expansion part is 92mm and the length of the contraction part is 30mm. The contour of the model is designed by the method of characteristic (MOC) and the angle at the exit is 0°.

https://doi.org/10.1017/S0001924000009192 Published online by Cambridge University Press

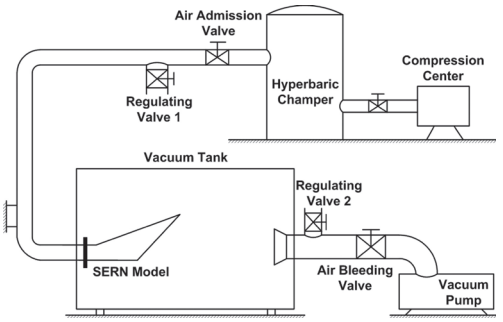

Figure 7. Sketch of the wind tunnel.

Figure 8. Blow down wind tunnel facility.

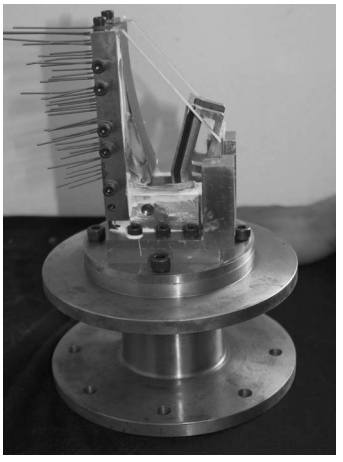

Figure 9. Photo of SERN model tested in the experiment.

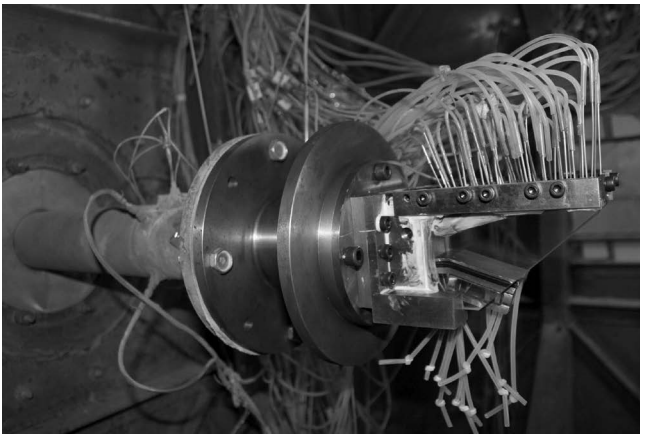

Figure 10. Photo of SERN model installed in the wind tunnel.

2.2 The separation transition in the startup process in the experiment

There are various separation patterns and the separation pattern transition occurs when the SERN model works in the process of the startup. At the beginning of the wind tunnel starting, the jet flows along the flap. When the main valve is turned on gradually, the total pressure at the inlet of the nozzle increases. Then the shock train becomes stronger. Figure 11(a) shows the jet flowing along the flap. When the total pressure is high enough, the jet jumps to the expansion ramp suddenly and the Mach stem appears in the flow field. Figure 11(b) shows the flow field after the transition of the separation pattern. The flow field changes tempestuously and the jet deflects the thrust direction, so the transition will make adverse impact to the SERN performance.

Although the different separation patterns and their transition process have been observed in the experiment, no further details could be provided for such a complex, unsteady flow field owing to the limitation of the test facilities. It is hard to describe it precisely only based on the experimental data at hand at the present time. While the numerical simulation can give the intuitive results and help to analyse and understand the phenomenon. Therefore, in the following, the separation patterns and effects of the separation pattern transition on the SERN's performance will be discussed based on the numerical simulations.

https://doi.org/10.1017/S0001924000009192 Published online by Cambridge University Press

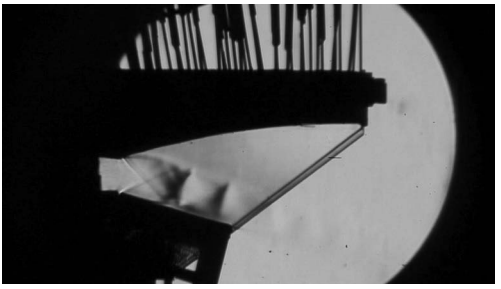

(a) RSS with the separation bubble forming on flap in startup process, operating *NPR* = 2·4.

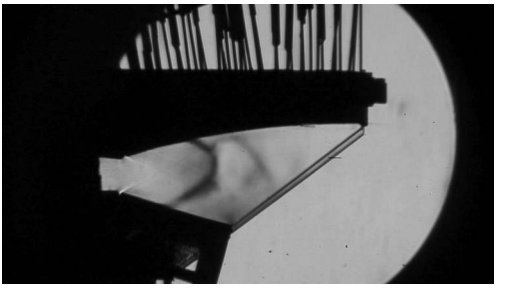

(b) RSS with the separation bubble forming on ramp in startup process, operating *NPR* = 2·6.

Figure 11. Different separation patterns in subscale SERN experiments.

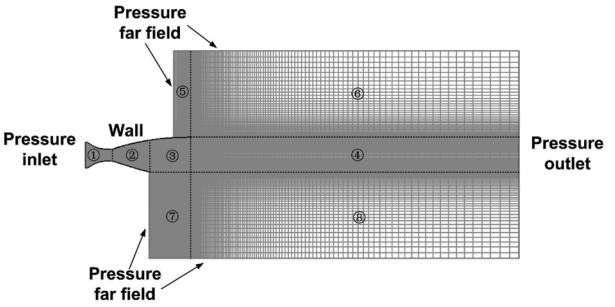

Figure 12. The grid case of the SERN for numerical simulation.

2.3 Experimental validation of numerical simulation method

The model is a subscale two-dimensional SERN with cold airflow through it. The density based solver is adopted in the simulation. The discretisation method is the second order upwind and the viscous model is *k*-ε turbulence model. The CFD results are computed by FLUENT software. The boundary conditions are set as in the experiment, and the *NPR* of the nozzle is 3·5. The boundary conditions for numerical simulation are showed in Fig. 12 and Table 1.

The geometry of the SERN has been meshed by Gambit with a structured mesh. The grid is shown in Fig. 6. The node distributions in the *x* and *y* directions of regions 1, 2, 3, 4, 5 and 7 are 80 × 80, 150 × 80, 150 × 80, 120 × 80, 40 × 50 and 150 × 50, respectively. The node distributions in regions 6 and 8 are 120 × 50. The y^+ in the simulation varies in the range 10-80. In the over-expanded flow field, the separation phenomena are complex. Separation and reattachment occurs

Table 1
Parameters of the SERN and the boundary conditions for numerical simulations

Parameters	**Data**
Expansion area ratio	3·07
Pressure inlet	P_t = 124,008·5Pa, T_1 = 296·5K
Pressure far field	P= 35,422·69Pa, T_1 = 296·5K, Ma = 0
Pressure outlet	P_t = 35,422·69Pa, T_1 = 296·5K

https://doi.org/10.1017/S0001924000009192 Published online by Cambridge University Press

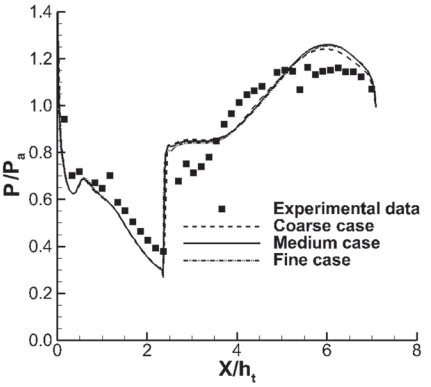

Figure 13. Wall pressure distribution of the test model.

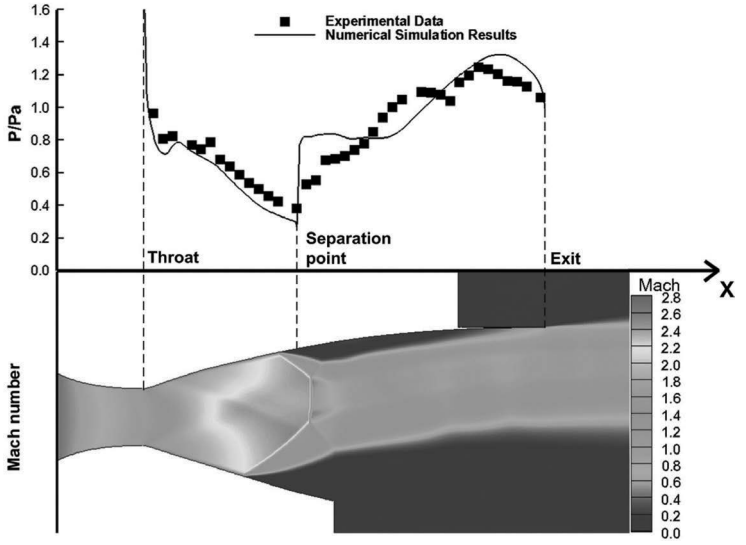

Figure 14. Numerical simulation results and experimental data validation.

in SERN and the flow speeds are quite different between the main jet and the separation bubble. As a result, the y^+ location varies to a large degree.

The grid case used above is defined as medium one, and the grid independence study has been conducted with the node distributions in the x and y directions being increased by a factor of 2 (fine) and decreased by a factor of 0·5 (coarse). The medium grid case constitutes the baseline as described above. The variability of the pressure on the expansion ramp between the three cases was within 3%, as shown in Fig. 13. As a result, the medium grid distribution was deemed suitable for further investigation. The numerical results for the over-expanded SERN are credible when the *NPR* of the nozzle is near 3.

Figure 14 shows the Ma flood contour and the pressure distributions of the expansion ramp. From the CFD results, it can be found the pressure distributions by the experiment and CFD method agree well with each other. The position of the separation point predicted by the numerical

https://doi.org/10.1017/S0001924000009192 Published online by Cambridge University Press

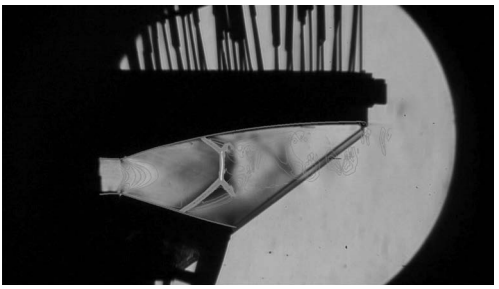

Figure 15. Schlieren photograph and CFD density gradient field of the SERN model for validation, operating *NPR* = 3·5.

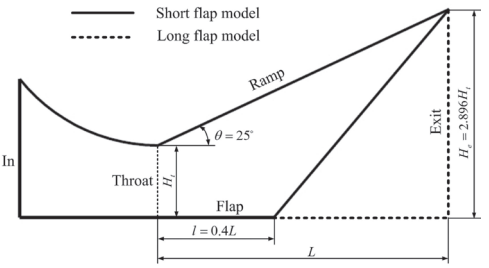

Figure 16. The configurations of short flap SERN and long flap SERN.

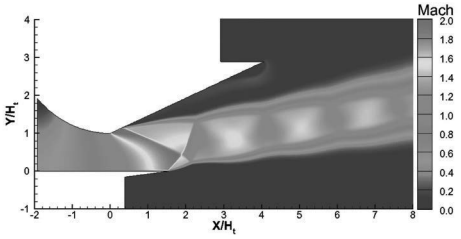

Figure 17. Ma flood contour of FSS in short flap SERN, operating *NPR* = 3·0.

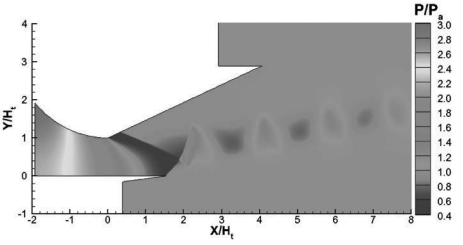

Figure 18. Static pressure flood contour of FSS in short flap SERN, operating *NPR* = 3·0.

simulation is almost the same as the experiment. The phenomenon of the reattachment is also observed in the numerical results. Moreover, the structures of the shock waves are well simulated by CFD method, with the separation shock waves, the Mach stem and the λ shock wave structures can be distinguished in Fig. 15, which is similar to the flow field showing in the Schlieren photo.

3.0 SEPARATION PATTERN OF SERN

3.1 FSS in SERN

In this paper, the straight expansion ramp SERN will be considered for investigation as it has a relatively simple design and the geometry of the nozzle can be easily controlled. In our simulation, the expansion area ratio is 2·896 and the expansion angle is 25º. The short flap SERN model and long flap SERN model will be discussed below and the nozzle configuration at different flap lengths is shown in Fig. 16.

FSS is a special separation pattern in SERN. The flow does not reattach to the wall any longer after the main flow separates from the expansion wall, which is like the behaviour of the free jet downstream of the separation point. There is no separation bubble in the flow field near to the expansion wall and the flap, and the ambient air will be entrained into the recirculation zone, so the pressure in the recirculation zone is near to the ambient pressure.

Figure 17 and Fig. 18 are, respectively, Mach number flood contour and static pressure flood contour of the FSS in SERN with short flap, where the length of the flap is only about 40% of the whole expansion wall length. If the flap is short enough, the flow separation does not appear on

https://doi.org/10.1017/S0001924000009192 Published online by Cambridge University Press

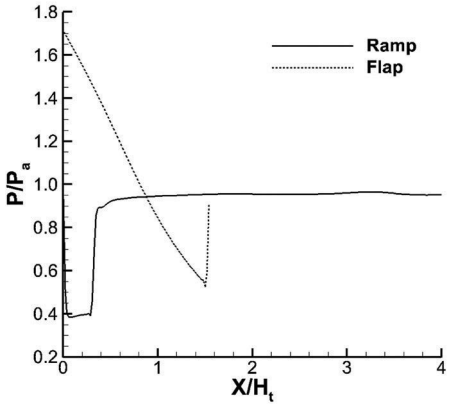

Figure 19. Pressure distributions on the ramp and the flap of short flap SERN, FSS, operating *NPR* = 3·2.

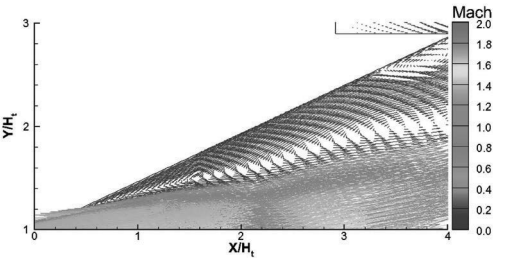

Figure 20. Velocity vector contour at the separation spot of FSS in short flap SERN, operating *NPR* = 3·0.

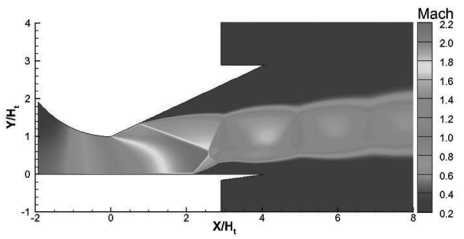

Figure 21. Ma flood contour of FSS in long flap SERN, operating *NPR* = 3·25.

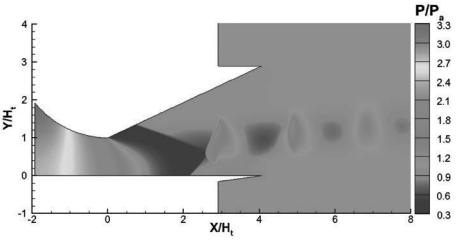

Figure 22. Static pressure flood contour of FSS in short flap SERN, operating *NPR* = 3·25.

the flap and the jet only separates from the expansion ramp. There is a shock at the trailing edge of the flap, which is generated owing to the abrupt pressure difference between the inner flow field and the ambient. Usually, the separation shock in the FSS is relatively weak comparing to the axisymmetric rocket nozzle, so the normal shock wave does not appear when the two shock waves intersect. Then, there is a shock train formed by expansion waves and compression waves that are similar to free jet. Because the reattachment does not appears in the nozzle, the ambient gas get into the recirculation zone on the expansion ramp and the pressure on the wall after the separation point is near to the ambient pressure. The pressure distributions on the wall are shown in Fig. 19 and the velocity vector contour at the separation spot is shown in Fig. 20.

Figure 21 and Fig. 22 are Mach number flood contour and static pressure flood contour of the FSS in SERN with long flap, respectively. The length of the flap is the same as the whole expansion wall length. In this case, the jet separates from both the expansion ramp and the flap under the serious over-expansion. The separation shocks are stronger than those in short flap SERN, and there might be a Mach stem when the two shock waves intersect with each other, so the two λ-shape shock wave structures appear in the flow field. While FSS is not a very stable status, the *NPR* range of FSS in long flap SERN is quite small, from 3·2378 to 3·3128, due to the Coanda effect. Similar to the FSS in short flap SERN, there is no attachment in FSS in the long flap model. The recirculation zones on ramp and flap are opened and the pressure in the recirculation is nearly the

https://doi.org/10.1017/S0001924000009192 Published online by Cambridge University Press

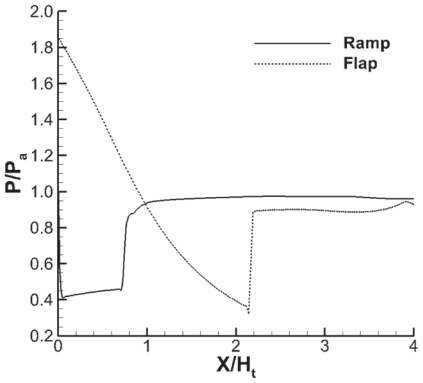

Figure 23. Pressure distributions on the ramp and the flap of long flap SERN, FSS, operating *NPR* = 3·25.

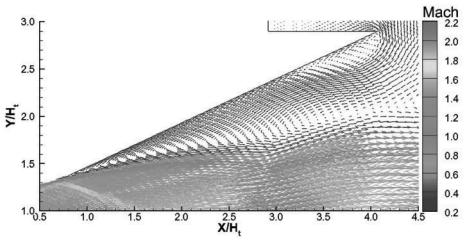

Figure 24. Velocity vector contour at the ramp separation spot of FSS in short flap SERN, operating *NPR* = 3·25.

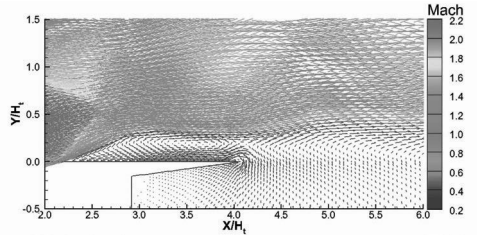

Figure 25. Velocity vector contour at the flap separation spot of FSS in short flap SERN, operating *NPR* = 3·25.

ambient pressure. The pressure distributions on the wall are shown in Fig. 23 and the velocity vector contour at the ramp and flap separation spot are shown in Figs 24 and 25 respectively.

The shape and the strength of the separation shock on the SERN expansion ramp and the flap are different, because it is asymmetrical, i.e., the expansion degrees on them are not the same. Therefore, in FSS pattern, the separation shock on expansion ramp is stronger than that on flap, and the λ-shape shock wave structure caused by separation shock on expansion ramp is larger and more obvious.

3.2 RSS in SERN

Figure 26 and Fig. 27 are Mach number flood contour and static pressure flood contour of the RSS in SERN with short flap as shown above, respectively. RSS is a common separation pattern in SERN. The separated main flow reattaches to the wall some distance downstream of the separation point, and the main jet seems to be restricted near to the wall. If the flap is short enough, the flow only can reattach to the expansion ramp. Because of the reattachment, there is a separation bubble in the flow field, and the exhaust air stream behind the shock will be entrained into the separation bubble, so the pressure in it is much higher than that on the separation point. The pressure distributions on the wall are shown in Fig. 28 and the velocity vector contour at the separation spot is shown in Fig. 29.

The critical *NPR* of the RSS in SERN with short flap is higher than that of FSS, and the normal shock wave might appear when the two shock waves intersect. When the short flap SERN operates

https://doi.org/10.1017/S0001924000009192 Published online by Cambridge University Press

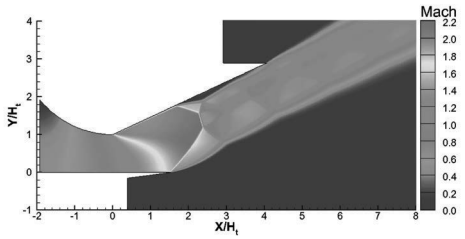

Figure 26. Ma flood contour of RSS in short flap SERN, operating *NPR* = 3·0.

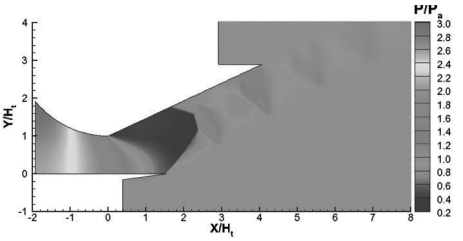

Figure 27. Static pressure flood contour of RSS in short flap SERN, operating *NPR* = 3·0.

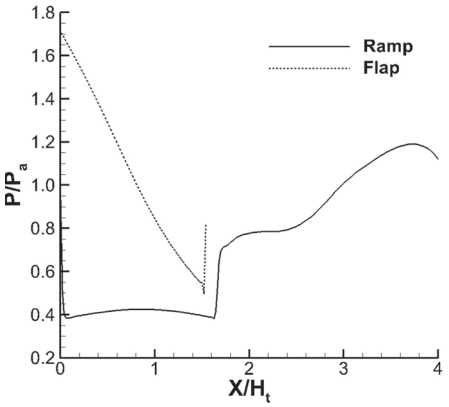

Figure 28. Pressure distributions on the ramp and the flap of short flap SERN, RSS, operating *NPR* = 3·0.

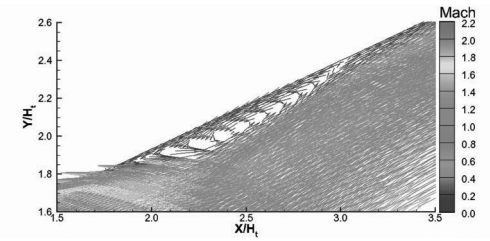

Figure 29. Velocity vector contour at the separation spot of RSS in short flap SERN, operating *NPR* = 3·0.

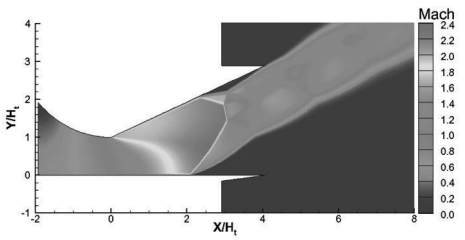

Figure 30. Ma flood contour of RSS with separation bubble on expansion ramp in long flap SERN, operating *NPR* = 3·4.

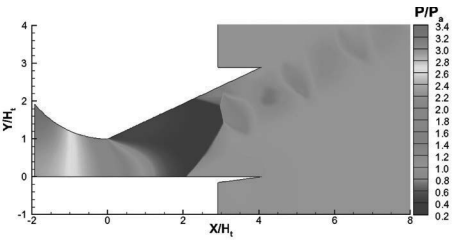

Figure 31. Static pressure flood contour of RSS with separation bubble on expansion ramp in long flap SERN, operating *NPR* = 3·4.

in RSS mode, the main jet will deviate from the thrust direction, which will affect the nozzle performance.

If the flap is long enough, the reattachment can happen not only on the expansion ramp but also on the flap. Figure 30 and Fig. 31 is respectively Mach number flood contour and static pressure flood contour of the RSS in SERN with long flap, with the separation bubble is restricted near to the expansion ramp. It is similar to the RSS in short flap, except there is a large recirculation

https://doi.org/10.1017/S0001924000009192 Published online by Cambridge University Press

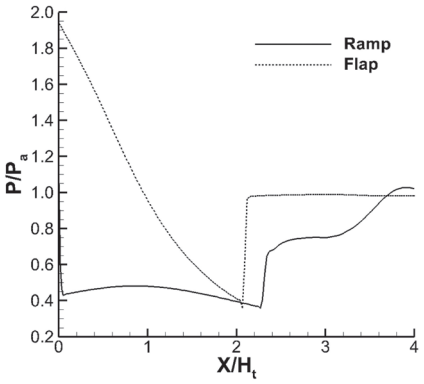

Figure 32. Pressure distributions on the ramp and the flap of long flap SERN, RSS with separation bubble on ramp, operating *NPR* = 3·4.

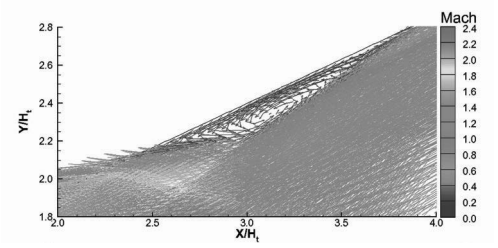

Figure 33. Velocity vector contour at the ramp separation spot of RSS with separation bubble on expansion ramp in long flap SERN, operating *NPR* = 3·4.

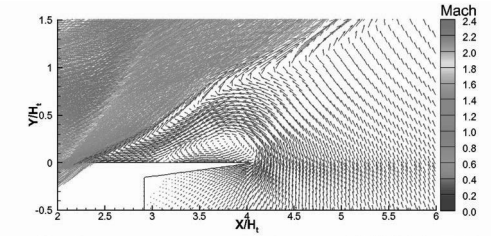

Figure 34. Velocity vector contour at the flap separation spot of RSS with separation bubble on expansion ramp in long flap SERN, operating *NPR* = 3·4.

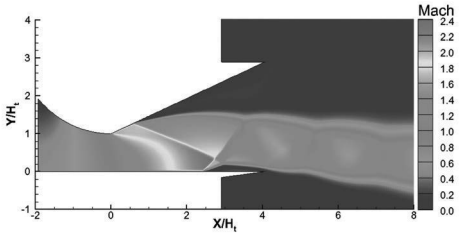

Figure 35. Ma flood contour of RSS with separation bubble on flap in long flap SERN, operating *NPR* = 3·2.

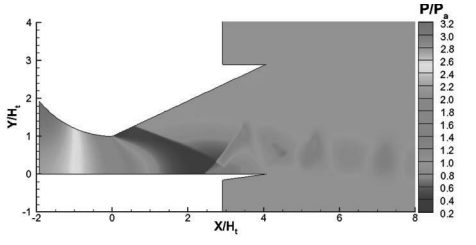

Figure 36. Static pressure flood contour of RSS with separation bubble on flap in long flap SERN, operating *NPR* = 3·2.

zone rather than separation bubble appears on the flap. Then the ambient air is entrained into the recirculation zone, and the pressure in the recirculation zone is almost the same as the ambient pressure. The pressure distributions on the wall are shown in Fig. 32 and the velocity vector contour at the ramp and flap separation spot are shown in Figs 33 and 34, respectively.

Figure 35 and Fig. 36 is Mach number flood contour and static pressure flood contour of the RSS in SERN with long flap as mentioned above, respectively. In this pattern, the separation bubble appears on the flap of SERN, and the recirculation zone on the expansion ramp is filled

https://doi.org/10.1017/S0001924000009192 Published online by Cambridge University Press

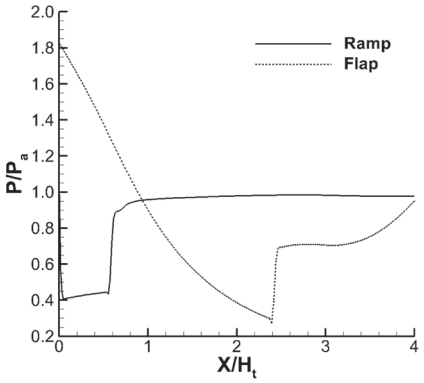

Figure 37. Pressure distributions on the ramp and the flap of long flap SERN, RSS with separation bubble on ramp, operating *NPR* = 3·2.

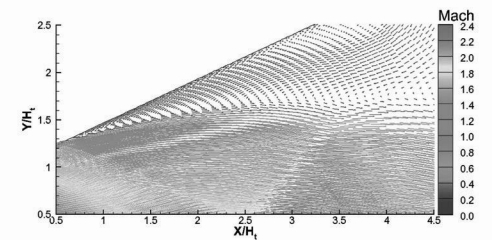

Figure 38. Velocity vector contour at the ramp separation spot of RSS with separation bubble on flap in long flap SERN, operating *NPR* = 3·2.

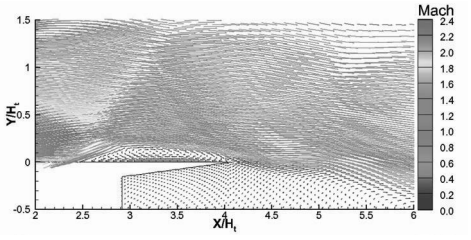

Figure 39. Velocity vector contour at the flap separation spot of RSS with separation bubble on flap in long flap SERN, operating *NPR* = 3·2.

by ambient air. The separation bubble leads to the pressure increase in it on the flap, and the main jet might be driven to turn downward the flap when the separation bubble is near the trailing edge of flap. The pressure distributions on the wall are shown in Fig. 37. When the long flap SERN works in RSS case with the separation bubble on the flap, there is no normal shock in the flow field, and the separation shock on flap is quite short, which results in the separation bubble to be very small. The velocity vector contour at the ramp and flap separation spot are shown in Figs 38 and 39, respectively.

In these patterns, almost all shock waves are oblique and the separation shock waves are the most important shock in the flow field. When the separation bubble is generated on the expansion ramp, the separation shock on the flap becomes stronger. And when the separation bubble is generated on the flap, the separation shock on the expansion ramp also becomes stronger.

4.0 SEPARATION PATTERN TRANSITION IN SERN

The separation pattern transition always happens in the process of startup and shutdown, and it just takes very little time. Separation pattern transition in SERN is an unsteady process, so the unsteady flow solver in the Fluent Software is adopted, and the user defined function (UDF) is used in the numerical calculation to simulate the total pressure change at the inlet of nozzle. In

https://doi.org/10.1017/S0001924000009192 Published online by Cambridge University Press

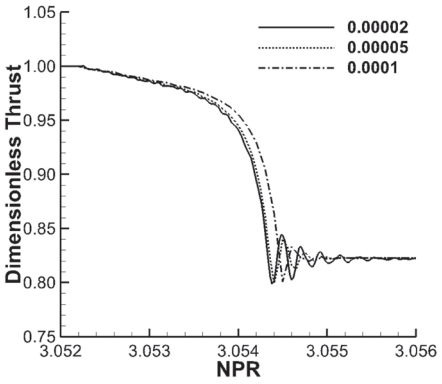

Figure 40. Thrust changes with different time steps during the FSS-to-RSS transition of the short flap SERN model.

the calculation, the time steps 0·0001s, 0·00005s and 0·00002s have been used to simulate the FSS-to-RSS transition of the short flap SERN model, with the length of the nozzle as 52·9mm, the maximum velocity in the nozzle as about 520ms^{-1}, and therefore the time-scale is about 0·0001s during the separation transition process. Figure 40 shows the results of thrust changes in the separation transition process with various time steps. It can be found from the figure that the thrust changes of different time steps are the same before and after the transition and the transition pressure ratios of 0·00005s and 0·00002s are almost the same, so the time step size 0·00005s has been chosen in the simulation and the maximum iterations per time step is 300.

The simulation results are discussed in the following. As mentioned above, the kind of the separation pattern that occurs in the over expanded SERN depends on not only the *NPR*, but also the relative length of the flap. So the separation pattern transitions problem will be discussed in short flap SERN at first, then in the long flap SERN.

4.1 Separation pattern transitions in short flap SERN

In the experiment, it can be found that the process of the separation last for a very short time, and it seems that the separation transition completes instantaneously from visual observation. Therefore, a suitable method is needed to show the flow field in the separation transition, and the numerical simulation is the practical and easy one. The *NPR* of the model changes 0·2 per second. The *NPR* changes slowly in order to prove that the separation transition is the inherent unsteady phenomena rather than caused by rapid changing of *NPR*.

The model for numerical simulation is a SERN with the length of flap as 40% of the nozzle length. The total pressure at the inlet is increased continuously to simulate the process of startup. The *NPR* of the FSS status is lower than that of the RSS status, so the separation pattern changes from FSS to RSS in the process of startup. In the transition, the jet jumps to the expansion ramp from the free jet status, then the main jet reattaches on ramp, and then the separation bubble appears. In the process of transition, the separation point moves downstream rapidly and a Mach stem is formed in the flow field. As a result, the shock wave appears and the jet deflects a large angle. The jet deflects the thrust direction and it makes negative effects on the performance of the SERN. From the results, it can be found that the transition begins at *NPR* = 3·052 and ends at *NPR* = 3·056. The transition lasts less than 0·02s and the Ma flood contours in the separation pattern transition process are shown in Fig. 41.

https://doi.org/10.1017/S0001924000009192 Published online by Cambridge University Press

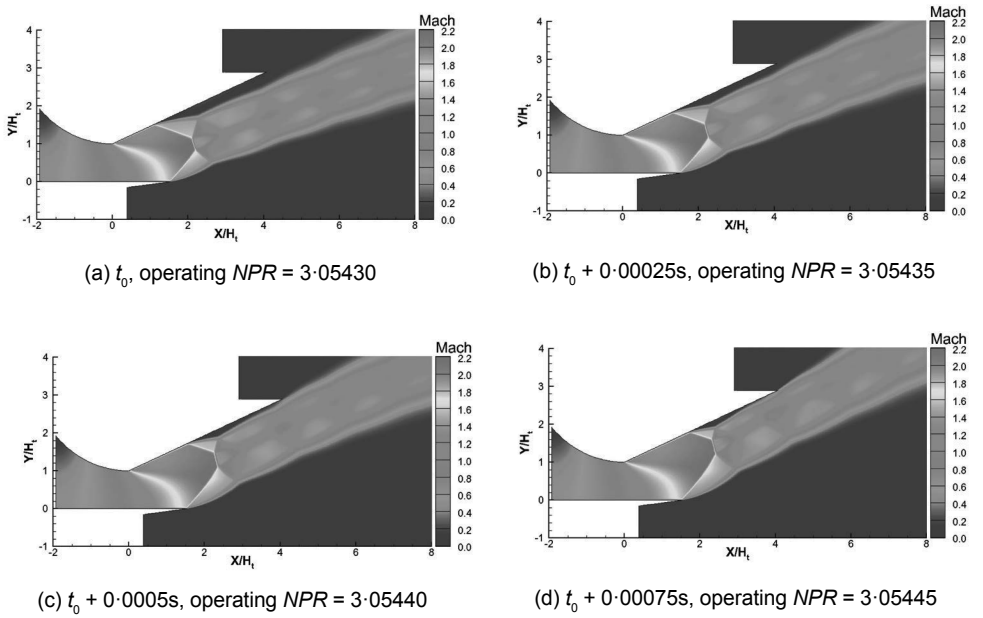

(a) t_0, operating *NPR* = 3·05430

(b) t_0 + 0·00025s, operating *NPR* = 3·05435

(c) t_0 + 0·0005s, operating *NPR* = 3·05440

(d) t_0 + 0·00075s, operating *NPR* = 3·05445

Figure 41. Ma flood contour of short flap SERN in FSS to RSS transition.

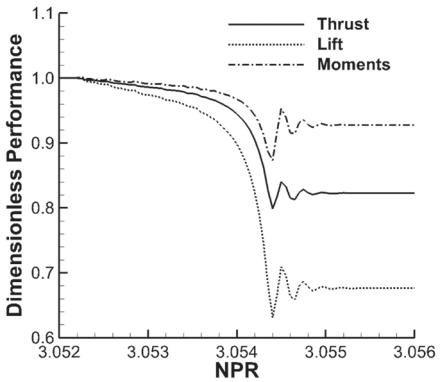

Figure 42. Performance of SERN from FSS to RSS in short flap.

Figure 42 is the changes of dimensionless performances such as the thrust, lift and moments in the separation pattern transition, which are non-dimensionalised by the thrust, lift and moments before the separation pattern transition. Thrust is calculated by the wall pressure and shear stress integration of the wet wall projected on *x* axis. Lift is calculated by projecting them on y axis. Moment caused by them is calculated corresponding to the intersection point of the throat and the flap. During the transition process of FSS to RSS, the thrust reduces 17·74%, the lift reduces 32·39% and moment reduces 7·24%. Due to the effect of the main jet impinging on the expansion wall in the transition process, the change of the performance reaches its peak in the transition, and the performance is stabilised after the oscillation. The maximum drops of thrust, lift and moment are 20·09%, 36·84% and 12·70%, respectively.

https://doi.org/10.1017/S0001924000009192 Published online by Cambridge University Press

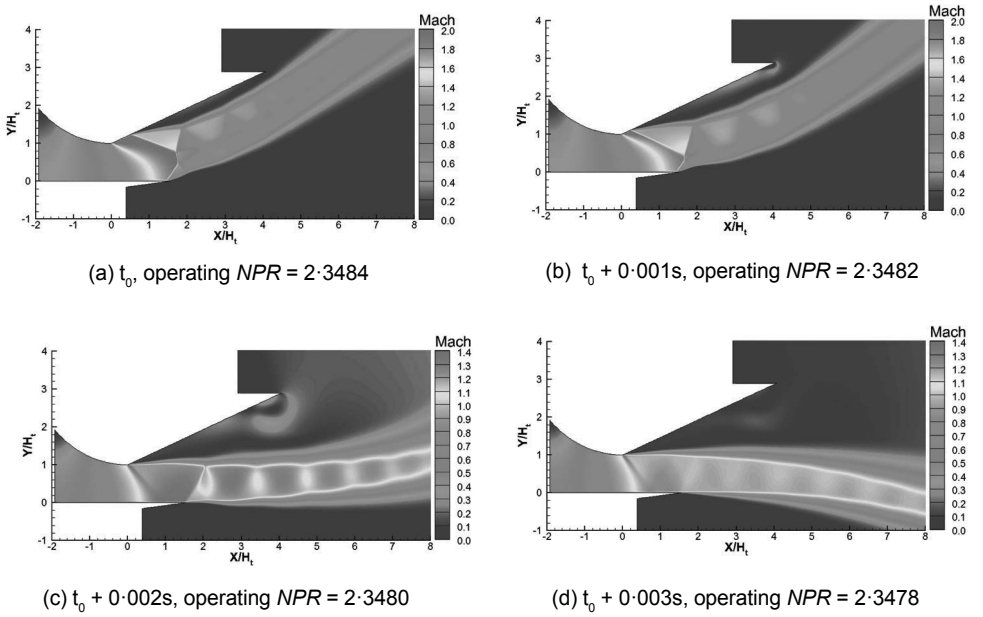

(a) t_0, operating *NPR* = 2·3484

(b) t_0 + 0·001s, operating *NPR* = 2·3482

(c) t_0 + 0·002s, operating *NPR* = 2·3480

(d) t_0 + 0·003s, operating *NPR* = 2·3478

Figure 43. Ma flood contour of short flap SERN in RSS to FSS transition.

After the FSS transfers to and stabilises as RSS, the total pressure at the inlet begins to decrease and the *NPR* decreases at a rate of 0·2/s. In the transition process of RSS to FSS, the critical *NPR* is lower than that of the process of FSS to RSS. As a result, the shock wave in the flow field is weaker. Before the separation transition happens, the separation bubble on the expansion ramp is quite large and the jet just reattaches at the trailing edge. The reattachment makes the separation bubble enclosed. But when the transition process is finished, the separation bubble opens to the surrounding and the ambient air get into the recirculation zone. The recirculation zone occupies almost all the expansion ramp, so the jet cannot expand enough on the ramp, and the velocity of the air is much lower than that before the transition. When the jet flows along the flap, it is similar to free jet and the direction of the jet is nearly along the thrust direction. Therefore, the performance of the SERN will get better after the RSS-to-FSS transition. The transition begins at *NPR* = 2·349 and ends at *NPR* = 2·347, with the transition process lasts less than 0·01s, and the Ma flood contours in the separation pattern transition process are shown in Fig. 43.

Figure 44 is the variations of the thrust, lift and moments in the separation pattern transition. In the process of RSS-to-FSS transition, the thrust increases 38·04%, the lift increases 59·62% and the moment increases 23·81%. The maximum raise of thrust, lift and moment is 46·52%, 68·20% and 29·85%, respectively. From the results, it can be found that the lift changes the most, just like the trend during the transition from FSS to RSS.

Comparing the SERN performance variation in the separation pattern transition process of FSS to RSS with that from RSS to FSS, it could be found that the performance changes more dramatically when the separation transfers from RSS to FSS. The pressure distributions on the expansion ramp have been extracted from the CFD results in order to analyse the reason of performance changing during the transition process. Figures 45 and 46 are respectively the pressure distributions on the expansion ramp in the processes of FSS transferring to RSS and RSS transferring to FSS. During the process of FSS transferring to RSS, the separation point moves downstream gradually with

https://doi.org/10.1017/S0001924000009192 Published online by Cambridge University Press

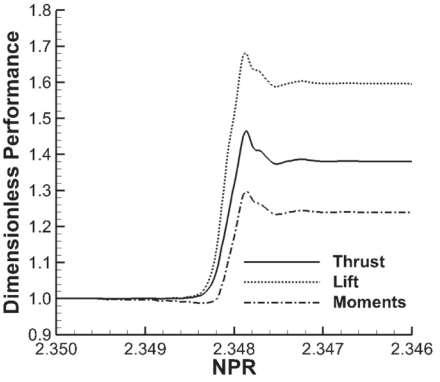

Figure 44. Performance of SERN from RSS to FSS in short flap.

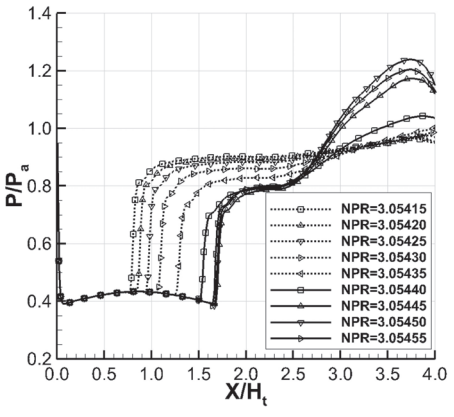

Figure 45. Pressure distributions on expansion ramp in FSS to RSS transition.

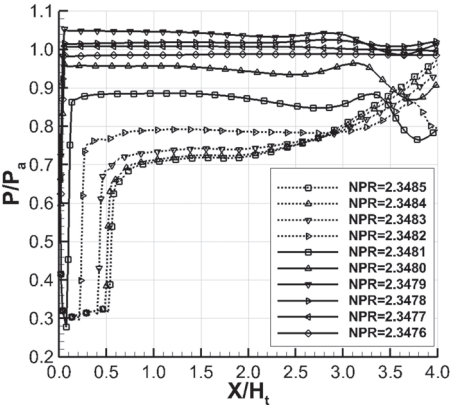

Figure 46. Pressure distributions in RSS to FSS transition.

the *NPR* increasing before the transition finally occurs, and the separation point moves about 0·9ht at the most. After the transition, the wall pressure in front of separation point on expansion ramp is much lower than the ambient pressure. As a result, the separation shock is weak and the pressure behind the separation point is not high enough. Therefore, the performance of the SERN reduces when the separation pattern transfers from FSS to RSS. In the process of RSS transferring to FSS, the phenomenon of separation pattern transition is the counterpart of the process of FSS transferring to RSS. The separation point moves upstream with the *NPR* decreasing before the transition finally occurs, and the separation point moves about 0·5ht at the most. The critical *NPR* of the RSS to FSS transition is lower than that of the FSS to RSS transition, so the separation point on the expansion ramp is nearer to the throat. Then the recirculation zone occupies almost all the expansion ramp, and the pressure on the ramp is near to ambient pressure. Therefore, the performance changes more greatly when the RSS to FSS transition happens.

From the computational results, it could be found that the critical transition *NPR* of FSS to RSS is about 3·0544, and the critical transition *NPR* of RSS to FSS is about 2·3481, so both the

https://doi.org/10.1017/S0001924000009192 Published online by Cambridge University Press

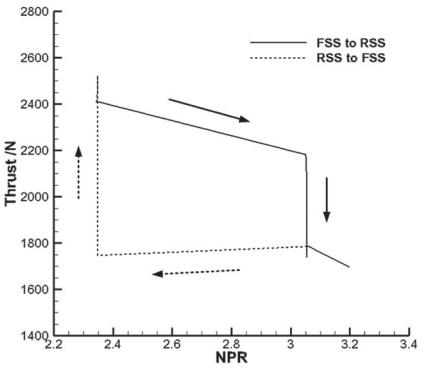

Figure 47. A hysteresis loop of thrust in SERN.

FSS and RSS are possible to occur in the *NPR* range of 2·3481 to 3·0544. As Fig. 47 shows, the difference of the critical *NPR* of the separation pattern transition leads to a hysteresis loop of the SERN performance, and method of active flow control could be used to improve the performance in the process of separation pattern transition.

The separation pattern transition is harmful to the nozzle performance and brings great challenges to the lifetime and the stability of SERN. In the future, the method to reduce the unfavourable influence on the SERN performance or even get rid of the transition should be studied.

4.2 Separation pattern transition in a long flap SERN

As mentioned above, there are two kinds of RSS in the long flap SERN: the separation bubble on expansion ramp, RSS(ramp), and the separation bubble on flap, RSS(flap). In the process of startup, the RSS(flap) transfers to FSS at first, then from FSS to RSS(ramp), and finally stabilises on the expansion ramp. However, in the process of shutdown, the FSS might disappear and the separation pattern transfers directly from the RSS(ramp) to the RSS(flap). Therefore, RSS is a stable separation pattern in long flap SERN rather than the stable one as FSS in the rocket nozzle.

When the *NPR* of long flap SERN is increased step by step, the transition of RSS(flap) to FSS happens firstly. In this process, the main jet turns upwards little by little, and the separation bubble on the flap is finally opened. As a result, the ambient air gets into the recirculation zone. From the numerical simulation, it can be found that the transition begins at the *NPR* 3·236 and ends at the *NPR* 3·24. Figure 48 shows the changes of the thrust, lift and moments during the transition process. It can be found that lift changes the most, then the moments, and the thrust changes the least. The thrust reduces 1·09%, the lift reduces 114·57% and the moment reduces 11·21%. And the direction of lift is reversed in the transition process. The pressure distributions on the expansion ramp and flap in the processes of RSS(flap) to FSS transition are shown in Fig. 49 and Fig. 50, respectively. Before the transition, the separation bubble is closed and the ambient gas cannot get into the separation bubble. When the separation completes, the separation bubble is opened and the ambient gas fills in the recirculation zone. The velocity vector contour at separation point is shown in Fig. 51.

Secondly, it is the transition from FSS to RSS(ramp). In this transition process, the main jet reattaches to the expansion ramp in a very short time and the separation point on the expansion ramp moves downstream rapidly. The flow direction of the jet changes a lot, hence the transition

https://doi.org/10.1017/S0001924000009192 Published online by Cambridge University Press

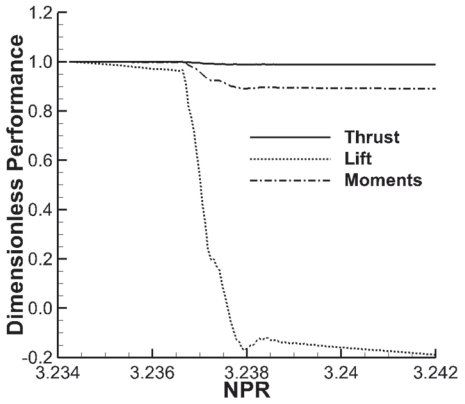

Figure 48. Performance changes of long flap SERN in RSS(flap) to FSS transition.

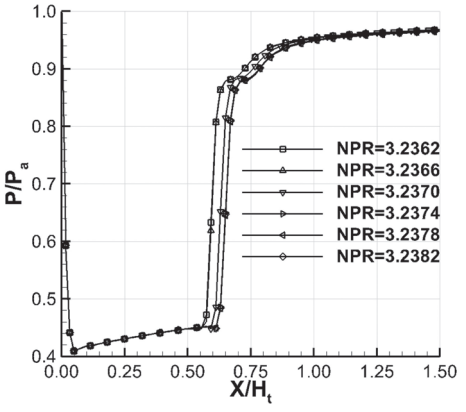

Figure 49. Pressure distributions on expansion ramp of long flap SERN in RSS(flap) to FSS transition.

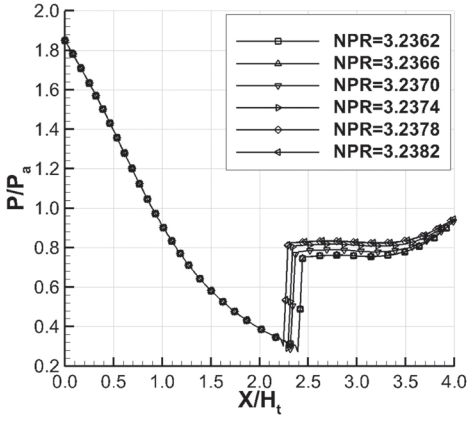

Figure 50. Pressure distributions on flap of long flap SERN in RSS(flap) to FSS transition.

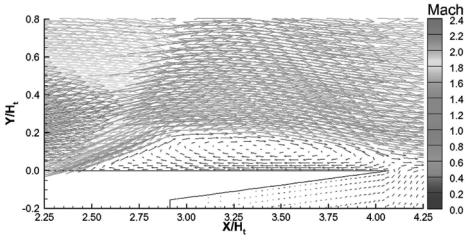

(a) t_0, operating *NPR* = 3·2362

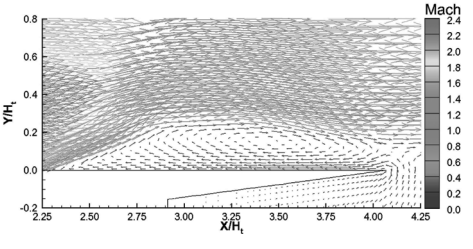

(b) $t_1 = t_0 + 0{\cdot}01$s, operating *NPR* = 3·2382

Figure 51. Velocity vector contour at separation point of long flap SERN in RSS(flap) to FSS transition.

https://doi.org/10.1017/S0001924000009192 Published online by Cambridge University Press

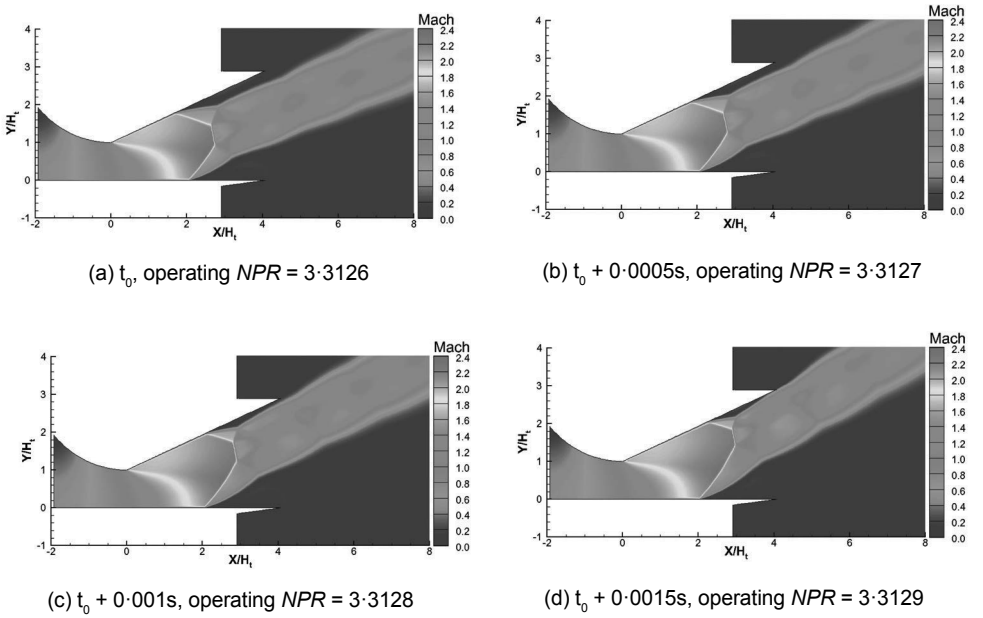

(a) t_0, operating *NPR* = 3·3126

(b) t_0 + 0·0005s, operating *NPR* = 3·3127

(c) t_0 + 0·001s, operating *NPR* = 3·3128

(d) t_0 + 0·0015s, operating *NPR* = 3·3129

Figure 52. Ma flood contour of long flap SERN in FSS to RSS(ramp) transition.

affects greatly on the performance of the SERN. From the numerical simulation, it can be found that the transition begins at the *NPR* 3·310 and ends at the *NPR* 3·314. The transition lasts less than 0·01s and the Ma flood contours in the separation pattern transition process are shown in Fig. 52.

Figure 53 shows the performance changes of the long flap SERN in the separation pattern transition from FSS to RSS(ramp). As shown in the figure, the lift changes the most and the thrust changes the least, which is different from the regularity in the transitions of short flap SERN. From the beginning to the end of the separation pattern transition, the thrust reduces 20·65%, the lift reduces 82·52% and the moment reduces 67·89%. For the peak of the changes at the instant of the transition, the thrust reduces 21·66%, the lift reduces 83·71% and the moment reduces 71·06%. Comparing with the FSS-to-RSS transition in short flap transition, the direction of the main jet changes less in the long flap SERN. Therefore, the effects of the impingement and the oscillation of the main jet become weaker.

When the *NPR* of the nozzle is decreased 0·2 per second in the numerical simulation, the transition process of RSS(ramp) to RSS(flap) begins at *NPR* = 2·357 and ends at *NPR* = 2·355. The transition lasts less than 0·01s and the Ma flood contours in the separation pattern transition process are shown in Fig. 54.

Figure 55 is the variations of the thrust, the lift and the moments in the separation pattern transition process, in which, the thrust increases 39·31%, the lift increases 100·08% and the moment increases 132·62%. The maximum growth of the thrust, the lift and the moment is respectively 53·39%, 105·15% and 154·54%. The transition *NPR* in long flap SERN is greater than that in short flap SERN.

Figure 56 shows the *NPR* range of each separation pattern and the transition point. It can be found that the long flap causes another separation pattern, RSS(flap), and the separation pattern transitions are different from those in short flap model. Moreover, the transition *NPR* of the SERN

https://doi.org/10.1017/S0001924000009192 Published online by Cambridge University Press

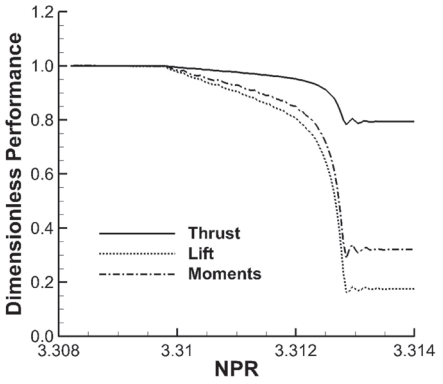

Figure 53. Performance of SERN from FSS to RSS(ramp).

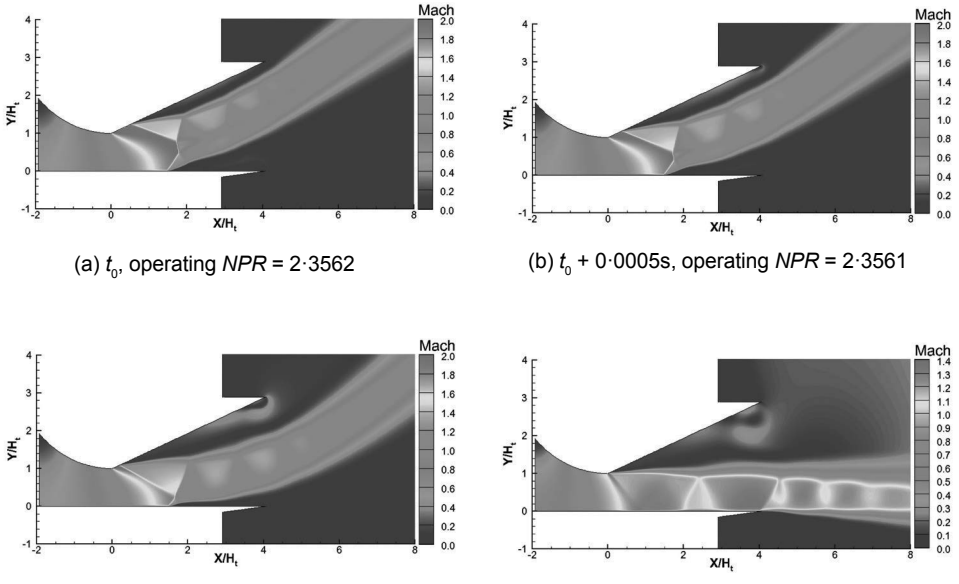

(a) t_0, operating *NPR* = 2·3562

(b) t_0 + 0·0005s, operating *NPR* = 2·3561

(c) t_0 + 0·001s, operating *NPR* = 2·3560

(d) t_0 + 0·002s, operating *NPR* = 2·3558

Figure 54. Ma flood contour of long flap SERN in RSS(ramp) to RSS(flap) transition.

with long flap is greater. In the long flap model, the FSS status occurs in the *NPR* from 3·2378 to 3·3128, which is a period in a twinkle in the startup process, so the FSS is not a stable status and the RSS is the main separation pattern in the long flap model. It is also noted that the length of the flap can affect the separation patterns and the transition *NPR*, even the performance of the SERN, when it works under over-expanded condition. Further research should be done to understand the influences caused by the length of the flap, and then to guide the design of the SERN under over-expanded condition in the future.

https://doi.org/10.1017/S0001924000009192 Published online by Cambridge University Press

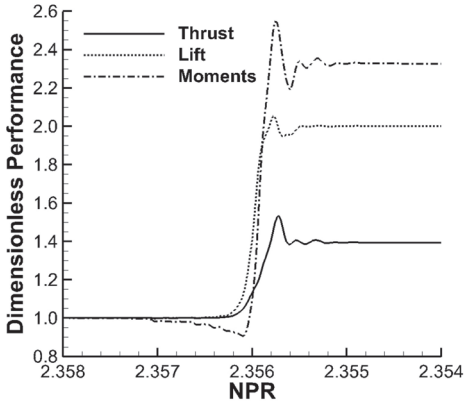

Figure 55. Performance of SERN from RSS(ramp) to RSS(flap).

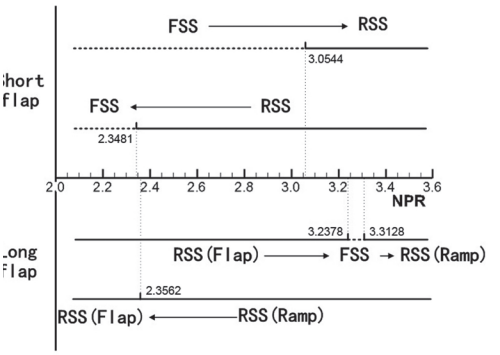

Figure 56. The separation pattern transition point and the *NPR* range of each separation pattern.

5.0 CONCLUSIONS

In the present paper, the different separation patterns and the separation pattern transition phenomena in the over-expanded SERN are shown. The intuitive results are helpful to analyse and understand the phenomena more thoroughly. Based on the study, it can be found that there are many differences between the separation patterns of SERN and the common axisymmetric rocket nozzle. The conclusions could be drawn as following:

1. Both FSS and RSS can occur in SERN, while RSS is the major and common separation pattern, which can be observed in almost all the SERNs. The separation bubble generated in the RSS is usually on the expansion ramp, but it may appear on the flap if the flap is long enough.
2. Oblique shock wave is the principal form of shock waves in the separation flow in SERN. The jet angle will change when the separation pattern transfers.
3. In the short flap SERN model, when the separation pattern transfers from FSS to RSS, the decreases of the thrust, the lift and the moment is 17·74%, 32·39% and 7·24%, respectively. And the increases of the thrust, the lift and the moment is 20·09%, 36·84% and 12·70%, respectively in the transition process of RSS to FSS.
4. From the computational results, it can be found that the lift changes the most and the SERN performance has a peak in the transition due to the dynamic effect of the jet impinging on the ramp.
5. The critical transition *NPR* of FSS to RSS transition is about 3·0544 and it is about 2·3481 for RSS to FSS transition. The difference of the separation pattern transition *NPR*s leads to a hysteresis loop of the SERN performance.
6. In the transition of RSS(flap) transferring to FSS, the flow field and the performance of the SERN do not change very much.
7. In long flap SERN during the process of shutdown, the FSS might disappear and the separation pattern might transfer directly from the RSS(ramp) to the RSS(flap).

https://doi.org/10.1017/S0001924000009192 Published online by Cambridge University Press

ACKNOWLEDGEMENTS

This work was supported by the National Natural Science Foundation of China (Grant No. 90916023), Funding of Jiangsu Innovation Program for Graduate Education (No. CXZZ13_0177) and Fundamental Research Funds for the Central Universities.

REFERENCES

1. HERRMAN, H. and RICK, H. Propulsion aspects of hypersonic turbo-ramjet engines with special emphasis on nozzle/aftbody integration, 1991, ASME Paper 91-GT-395.
2. ALBERTSON, C.W., EMAMI, S and TREXLER, C.A. Mach 4 test results of a dual-flow path, turbine based combined cycle inlet, 2006, AIAA paper 2006-8138.
3. HAID, D. and GAMBLE, E. Nozzle aftbody drag reduction using fluidics, 2004 AIAA paper 2004-3921.
4. XU, J.L. SHA, J. SHI, Z.Y. and ZHANG K.Y. PIV experimental study and numerical simulation of the over-expanded SERN exit jet, 2008, AIAA paper 2008-99.
5. GAMBLE, E. and HAID, D. Improving off-design nozzle performance using fluidic injection, 2004, AIAA paper 2004-1206.
6. GE, J.H, XU, J.L. WANG, M.T. and MO, J.W. prediction of flow separation in asymmetric ramp nozzle, *Acta Aeronautica et Astronautics Sinica*, 2012, **33**, (8), pp 1394-1399.
7. FREY, M and HAGEMANN, G. Flow separation and side-loads in rocket nozzles, 1999, AIAA paper 99-2815.
8. NAVE, L.H. and COFFEY, G.A. Sea level side loads in high-area-ratio rocket engines, 1973, AIAA paper 73-1284.
9. SCHMUCKER, R. Flow processes in overexpanded nozzles of chemical rocket engines, 1973, Report TB-7,-10,-14, Technical University Munich.
10. FREY, M. and HAGEMANN, G. Status of flow separation prediction in rocket nozzles, 1998, AIAA paper 98-3619.
11. FREY, M and HAGEMANN, G. Restricted shock separation in rocket nozzles, *J Propulsion and Power*, 2000, **16**, (3), pp 478-484.
12. FREY, M., HAGEMANN, G. and KOSCHEL. W. Appearance of restricted shock separation in rocket nozzles, *J Propulsion and Power*, 2002, **18**, (3), pp 577-584.
13. OSTLUND, J., DAMGAARD, T. and FREY, M. Side-Load phenomena in highly overexpanded rocket nozzles, *J Propulsion and Power*, 2004, **20**, (4), pp 695-704.
14. WATANABE, Y., SAKAZUME, N and TSUBOI, M. LE-7A engine nozzle problems during the transient operations, 2002, AIAA paper 2002-3841.
15. WATANABE, Y., SAKAZUME, N., YONEZAWA, K. and TSUJIMOTO, Y. LE-7A engine nozzle flow separation phenomenon and the possibility of RSS suppression by the step inside the nozzle, 2004, AIAA paper 2004-4014.
16. NASUTI, F., ONOFRI, M. and MARTELLI, E. Numerical analysis of flow separation structures in rocket nozzles, 2007, AIAA paper 2007-5473.
17. KWAN, W. and STARK, R. Flow separation phenomena in subscale rocket nozzles, 2002, AIAA paper 2002-4229.
18. WANG, T.S. Transient two-dimensional analysis of side load in liquid rocket engine nozzles, 2004, AIAA paper 2004-3680.
19. WANG, T.S., LIN, J., RUF, J. and GUIDOS, M. Transient three-dimensional side load analysis of out-of-round film cooled nozzles, 2010, NASA report M10-0136.
20. REIJASSE, PH., MORZENSKI, L., BLACODON, D. and BIRKEMEYER J. Flow separation experimental analysis in overexpended subscale rocket-nozzles, 2001, AIAA paper 2001-3556.
21. VERMA, S.B. and HAIDN, O. Study of restricted shock separation phenomena in a thrust optimized parabolic nozzle, *J Propulsion and Power*, 2009, **25**, (5), pp 1046-1057.
22. BROWN, A.M., RUE, J.H. and MCDANIELS, D.M. Recovering aerodynamic side loads on rocket nozzles using quasi-static strain-gage measurements, 2009, NASA report M09-0447.
23. RUF, J.H., MCDANIELS, D.M. and BROWN, A.M. Nozzle side load testing and analysis at Marshall Space Flight Center, 2009, AIAA paper 2009-4856.
24. RUF, J.H., MCDANIELS, D.M. and BROWN, A.M. Details of side load test data and analysis for a truncated ideal contour nozzle and a parabolic contour nozzle, 2010, AIAA paper 2010-6813.
25. BAARS, W.J. and TINNEY, C.E. Wall pressure unsteadiness and side loads in overexpanded rocket nozzles, *AIAA J*, 2012, **50**, (3), pp 61-73.